Catalysis Science & Technology

PAPER

View Article Online
View Journal | View Issue

Cite this: *Catal. Sci. Technol.*, 2014, 4, 387

Aqueous-phase reforming of xylitol over Pt/C and Pt/TiC-CDC catalysts: catalyst characterization and catalytic performance

Alexey V. Kirilin,[a] Benjamin Hasse,[b] Anton V. Tokarev,[a] Leonid M. Kustov,[c] Galina N. Baeva,[c] Galina O. Bragina,[c] Aleksandr Yu. Stakheev,[c] Anne-Riikka Rautio,[d] Tapio Salmi,[a] Bastian J. M. Etzold,[b] Jyri-Pekka Mikkola[ae] and Dmitry Yu. Murzin*[a]

Received 26th August 2013,
Accepted 4th November 2013

DOI: 10.1039/c3cy00636k

www.rsc.org/catalysis

The aqueous phase reforming (APR) of xylitol was studied over five Pt/C catalysts. The correlation between physico-chemical properties of the catalysts and catalytic performance was established. The Pt/C catalysts have different textural properties as well as different mean Pt cluster sizes and surface acidity. The average Pt cluster size was investigated by means of CO chemisorption as well as by TEM. The reaction was found to be structure sensitive and TOF linearly increases with increasing average Pt cluster size in the studied domain. The catalysts which possess higher surface acidity favoured higher rates of hydrocarbon production. On the contrary the Pt/C materials with lower acidities generated hydrogen with high selectivity and TOF.

Introduction

Sustainable evolution of our society is impossible without constant progress in such areas as chemical engineering and technology. In the context of a sustainable society biomass and biomass-derived products in the form of ready-to-use chemicals are attracting a lot of attention all over the world.[1,2] Hereby, much scientific effort was recently put into investigation of aqueous phase reforming (APR).[3]

APR is an important heterogeneously catalyzed reaction which can be used for production of hydrogen and alkanes. Because of that, APR has gained a lot of interest as a potential hydrogen and/or alkane supply from renewable biomass, therefore being an alternative to fossil fuels. APR is the process for transformation of aqueous solutions of polyols (such as ethylene glycol,[4–11] glycerol,[12–19] xylitol[20,21] or sorbitol[22–26]) and alcohols (methanol,[27,28] ethanol[28–30]). Numerous publications can be readily found on ethylene glycol (EG), glycerol and alcohol reforming. However, the number of scientific contributions devoted to APR of sugar alcohols is significantly less. The main reason for the latter case is a complicated product analysis, since for APR of xylitol or sorbitol more than 25 products are present in the liquid phase[25,31] in non negligible amounts.

The reaction is generally performed at elevated pressures (29–50 bar) and temperatures (498–523 K). Typically, the reaction pressure is 4 bar above the boiling point of water at a chosen process temperature. Various metals and support materials have been tested for the catalytic activity in APR[32] and so far Pt is the most used and studied metal possessing the highest catalytic activity and selectivity towards the desired products (hydrogen[33] or alkanes[34]). Depending on the support material and the process conditions (pH, acid additives), the reaction can be steered towards enhanced hydrogen or hydrocarbon formation. Different metal oxides[4,14,18,32,35,36] can be used as a support for Pt particles in the APR along with zeolites[21,23,37] and carbon.[12,32,38] Carbon supports for Pt catalysts in the APR process have recently attracted much scientific attention. Such carbon supports as Vulcan active carbon (Pt[12,32,38,39] and Pt–M, M = Re, Ru, Os, Fe, Cu, Sn, Ir[15]), activated carbon (Pt,[23,40,41] Pt–Re[42,43]), carbon fibers (Pt and Pt–Ru),[44] single-walled carbon nanotubes SWNTs (Pt and Pt–Co),[45–48] ordered mesoporous carbon CMK-3 (Pt,[49] Pt–Mn,[50] Pt–Re[51]) have been successfully investigated in the APR of polyols. These supports possess high hydrothermal stability under APR conditions (compared to the most investigated catalysts Pt on γ-Al_2O_3, where the alumina support might slowly transform into boehmite during water exposure at elevated temperatures and pressures[35,52]), large surface area and good

[a] *Laboratory of Industrial Chemistry and Reaction Engineering, Process Chemistry Centre, Åbo Akademi University, Biskopsgatan 8, FI-20500 Åbo-Turku, Finland. E-mail: dmurzin@abo.fi; Fax: +358 2 215 4479*
[b] *Institute of Chemical Reaction Engineering, University Erlangen-Nuremberg, Egerlandstraße 3, DE-91058 Erlangen, Germany*
[c] *Zelinsky Institute of Organic Chemistry, Leninsky prosp. 47, RU-119991, Moscow, Russia*
[d] *Microelectronics and Materials Physics Laboratories EMPART Research Group of Infotech Oulu, University of Oulu, FI-90014 Oulu, Finland*
[e] *Technical Chemistry, Department of Chemistry, Chemical Biological Centre, Umeå University, SE-901 87 Umeå, Sweden*

activity and hydrogen selectivity *via* APR. Nevertheless, there are not enough systematic studies devoted to investigation of the activity of Pt on different types of carbon supports. Moreover, some important carbon materials such as Sibunit,[53] which find a number of industrial applications, have not been investigated at all. Sibunit is a synthetic carbon composite, which is produced by pyrolysis of light hydrocarbons on a granulated carbon black followed by steam activation at 973–1123 K of the composite obtained.[54,55] A sponge-like system including meso- and macropores whose dimensions depend on the dispersion of the initial carbon black is formed. Sibunit is a class of porous carbon composite materials combining advantages of graphite (chemical stability and electric conductivity) and mesoporous active carbon (high specific surface area and mesopore volume). Therefore, this material is an attractive support for the preparation of Pt catalysts. The catalysts supported on Sibunit have been thoroughly investigated in many reactions, including hydrogenation and decarboxylation of fatty acids[56–58] and hydrogenation[59] and oxidation of volatile organic compounds.[60]

Additionally, our focus was also on carbide-derived carbons. The carbide-derived carbon (TiC-CDC) method allows one to synthesize nanoporous carbons with highly reproducible material properties. Hereby, *e.g.* pore size and pore volume, specific surface area and carbon morphology can be tailored towards special needs.[61–63] These features make TiC-CDC a promising model material in several fields of application, such as supercapacitors, gas-storage and separation and as a tailored catalyst support.[64–68]

Yet there is a lack of knowledge of the carbonaceous catalyst features influencing selectivity and yield of the desired products.[32] Moreover, it is worth noting that APR of such an important substrate as xylitol has not yet been studied over Pt/C catalysts. In addition, there are no systematic investigations of APR of polyols revealing the influence of the Pt cluster size on the reaction of higher polyols originating from biomass. It has been shown by Lehnert and Claus[13] that the Pt cluster size has a dramatic effect on hydrogen production from glycerol. The catalysts with bigger Pt clusters supported on alumina demonstrated higher TOF values in terms of the hydrogen production. A recent study by Kim *et al.*[49] showed that in the case of Pt catalysts supported on carbonaceous CMK the hydrogen production rate in APR of ethylene glycol increases with an increase of the metal loading. Structure sensitivity was therefore observed for C_2–C_3 polyols only. For the first time, this phenomenon has been described in the present work for polyols $>C_3$. On top of that, there is no systematic study explicitly demonstrating influence of surface acidity of Pt/C on APR of polyols.

The main purpose of the present work was thus preparation, characterization of various Pt/C catalysts (supported on TiC-CDC, Sibunit, active carbon (AC) and birch active carbon (BAC)) and investigation of their catalytic performance in APR of xylitol. Another goal was to correlate the catalytic results and the physico-chemical properties of the utilized materials.

Results and discussion

The textural properties of the Pt/C catalyst studied utilized in the present work study are summarized in Table 1.

Pt/BAC as well as Pt/C (Degussa) possess large surface areas exceeding 900 $m^2\ g^{-1}$. Pt/TiC-CDC has a surface area of 850 $m^2\ g^{-1}$. The Pt/Sibunit catalysts prepared from $(NH_3)_4Pt(HCO_3)_2$ (denoted as Pt/Sibunit (I)) and H_2PtCl_6 (denoted as Pt/Sibunit (II)) precursors have specific surface areas of 339 and 408 $m^2\ g^{-1}$, respectively. As can be noticed, the Pt/TiC-CDC sample has the largest pore volume of 0.61 $cm^3\ g^{-1}$ among the catalysts tested; Pt/C (Degussa) and Pt/Sibunit (I) have similar pore volumes: 0.52 and 0.53 $cm^3\ g^{-1}$, respectively. Meanwhile, Pt/BAC has a slightly lower pore volume than Pt/Sibunit (II) (0.47 and 0.45 $cm^3\ g^{-1}$), as can be seen from Table 1. Pt/TiC-CDC as well as Pt/C (Degussa) possess average pore diameters in the range of 1.2–1.5 nm, whereas Pt/Sibunit (I) and Pt/Sibunit (II) samples have mean pore sizes of 2.9 and 2.6 nm, respectively.

The average size of Pt clusters deposited on carbon supports was investigated by means of pulse CO chemisorption. The data are presented in Table 1. As can be seen, the size of the Pt cluster for all the catalysts was below 10 nm. Pt/TiC-CDC and Pt/Sibunit (I) have an average metal cluster size of 9.0 nm which corresponds to the metal dispersion of 12%. The Pt/Sibunit (II) catalyst prepared from H_2PtCl_6 has an average metal cluster size of 2.8 nm (metal dispersion = 41%). The difference in metal cluster sizes prepared from different metal salts shows that the metal precursor has an impact on the dispersion of the final catalyst. A slightly higher dispersion (47%) was calculated for Pt/C (Degussa) which corresponds to the mean Pt particle size of 2.4 nm. The highest dispersion was observed in the case of the Pt/BAC catalyst which has an average Pt cluster size of 1.5 nm and metal dispersion of

Table 1 Textural and surface properties of the Pt/C catalysts

Catalyst	Pt content, wt.%	Surface area, $m^2\ g^{-1}$	Pore volume, $cm^3\ g^{-1}$	Mean pore diameter, nm	CO uptake, $\mu mol\ g_{cat}^{-1}$	d_{Pt},[a] nm	D(Pt),[a] %
Pt/TiC-CDC	2.8	850	0.61	1.4	18.3	9.0	12
Pt/C (Degussa)	5	910	0.52	1.5	119.6	2.4	47
Pt/Sibunit (I)	5	339	0.53	2.9	31.3	9.0	12
Pt/Sibunit (II)	5	408	0.47	2.6	104.5	2.8	41
Pt/BAC	5	890	0.45	1.2	191.5	1.5	73
Pt/Al_2O_3	5	110	0.25	8.2	74.6	3.9	29

[a] Calculated based on the information provided by CO chemisorption.

73%. Generally, the larger surface area of the support facilitates the formation of smaller particles. However, as can be seen from Table 1, both the type of the carbon support and choice of the metal precursor contribute significantly to the final properties of the catalyst. Furthermore, there are such parameters as the point of zero charge (PZC), pH of deposition, and more specifically the driving force during the metal deposition [(PZC − pH)/PZC], which can also have an influence on the properties of the catalytic materials.

All Pt/C catalysts were examined by means of transmission electron microscopy (TEM) to determine the platinum cluster size distribution on the carbon surface and to compare the data with average cluster sizes obtained by CO chemisorption to TEM.

The TEM images of all the catalysts as well as corresponding particle size distributions are shown in Fig. 1. All the materials showed monomodal and narrow distribution of nanoparticles. The data obtained by TEM are in good agreement with the data obtained by pulse CO chemisorption (Table 2) except for two samples: Pt/TiC-CDC and Pt/Sibunit (I). For these exceptions, the average cluster sizes calculated on the basis of CO chemisorption data are higher than those obtained from TEM. Minor deviations in the mean Pt cluster values obtained by two different techniques can be caused by several reasons.

For example, bigger Pt clusters are difficult to identify when they melt and vanish into the background, especially in the case of carbon supported catalysts, or when overlaying smaller clusters melt in a bigger one. Moreover, during TEM imaging selected parts of the catalytic surface are imaged for calculations of the mean particle size and often do not represent the whole particle size distribution. On the contrary, chemisorption provides the total volume of the carbon monoxide adsorbed by Pt particles; therefore, all the particles capable of adsorbing CO are taken into account. Recently the similar issues were addressed by Wang *et al.*[46,48] The values for average Pt cluster size calculated from hydrogen and CO chemisorption were much higher compared to the results obtained by TEM and EXAFS. For instance, in a case of the Pt/MWNT-r (multi-wall nanotubes) catalyst the Pt particle size calculated from CO chemisorption was 5.26 nm, whereas it was 2.2 ± 1.2 and 2.3 ± 1.4 nm according to EXAFS and TEM, respectively. Moreover, Borchardt *et al.*[65] reported Pt cluster size determined by TEM to be 2.5 ± 0.6 nm, whereas CO chemisorption data provided an even smaller average cluster size of 1.5 nm, hence, both cases might take place. The authors partially explained the disagreement in the results obtained using different techniques by the fact that some Pt particles cannot be "chemically" seen by probe molecules. Another reason was a possible blocking of pores by larger particles. Additionally partially reduced metal clusters can be seen in TEM; however, they are not active in chemisorption of CO. In our case, for example, disagreement between CO chemisorption and TEM results was observed for two samples: Pt/TiC-CDC and Pt/Sibunit (I). Carbide-derived carbons are microporous materials with a narrow pore size distribution.[69] The Pt/TiC-CDC has an average pore size of 1.4 nm. Therefore, pore blocking might be the reason for the lower dispersion observed by TEM similar to that of Pt/MWNT described by Wang *et al.*[46] Nevertheless, a final conclusion regarding a discrepancy between two methods cannot be drawn due to the influence of many factors described above. As for Pt/Sibunit (I), the discrepancy can be caused by melting of the Pt particles into the background. This in turn complicates the identification of metal particles and correct size determination. Additionally, for both catalysts prepared from ammonia containing the Pt precursor the discrepancy between CO chemisorption and TEM data was observed. Probably, both materials are not completely reduced therefore higher values are obtained by CO titration compared to TEM analysis. Following the approach of Wang *et al.*,[46] all turnover frequencies are calculated on the basis of chemisorption data. This technique is considered to be more relevant for catalysis compared to TEM data.

Temperature-programmed reduction (TPR) profiles of the Pt/C catalysts are shown in Fig. 2. The catalysts after preparation were reduced using various techniques. The data are provided in the Experimental section. However, as can be seen from the TPR curves formation of Pt oxide species may occur. High-temperature hydrogen consumption peaks above 573 K can be assigned to hydrogen spill-over. Another reason for it might be high temperature reduction (>573 K) of the functional groups present on the carbon surface. Similar hydrogen consumption zones were observed for Pt/CMK catalysts.[51] Uptake of hydrogen was very low in the case of Pt/BAC, since during preparation this catalyst was reduced chemically by HCOOH. During storage Pt is partially oxidized as revealed by the TPR curve: the peak at 398 K corresponds to the reduction of PtO_x species. Prior to all the experiments the catalysts were pre-reduced under hydrogen flow for two hours at 523 K. Therefore, the Pt oxidation state for all the Pt/C catalysts can be regarded as Pt(0). However, Pt can interact with graphene sheets in CDC. Foley and co-workers reported that electron-rich graphene sheets interact with Pt nanoparticles and thus stabilize them.[70]

Acidic properties of the materials were investigated by NH_3-TPD. For each sample five NH_3-TPD curves at different heating rates were recorded to calculate the total amount of NH_3 adsorbed and the heat of ammonia desorption. The typical experimental curves recorded are shown in Fig. 3 for the Pt/C (Degussa) catalyst.

The data obtained for the Pt/C catalysts are summarized in Table 3, showing that different Pt catalysts possess different acidic properties and heats of ammonia desorption.

Rather low values of the heats of desorption indicate that all the catalysts possess weak acidic sites. As shown in Fig. 3a for Pt/C (Degussa), the temperature of the peak maximum (T_p) of ammonia desorption does not exceed 379 K which implies that the catalyst does not contain strong acid sites or acid sites of the moderate strength.[71] However, the Pt/C catalysts demonstrated differences in heats of NH_3 desorption and in the total amount of NH_3 desorbed, thus indicating minor

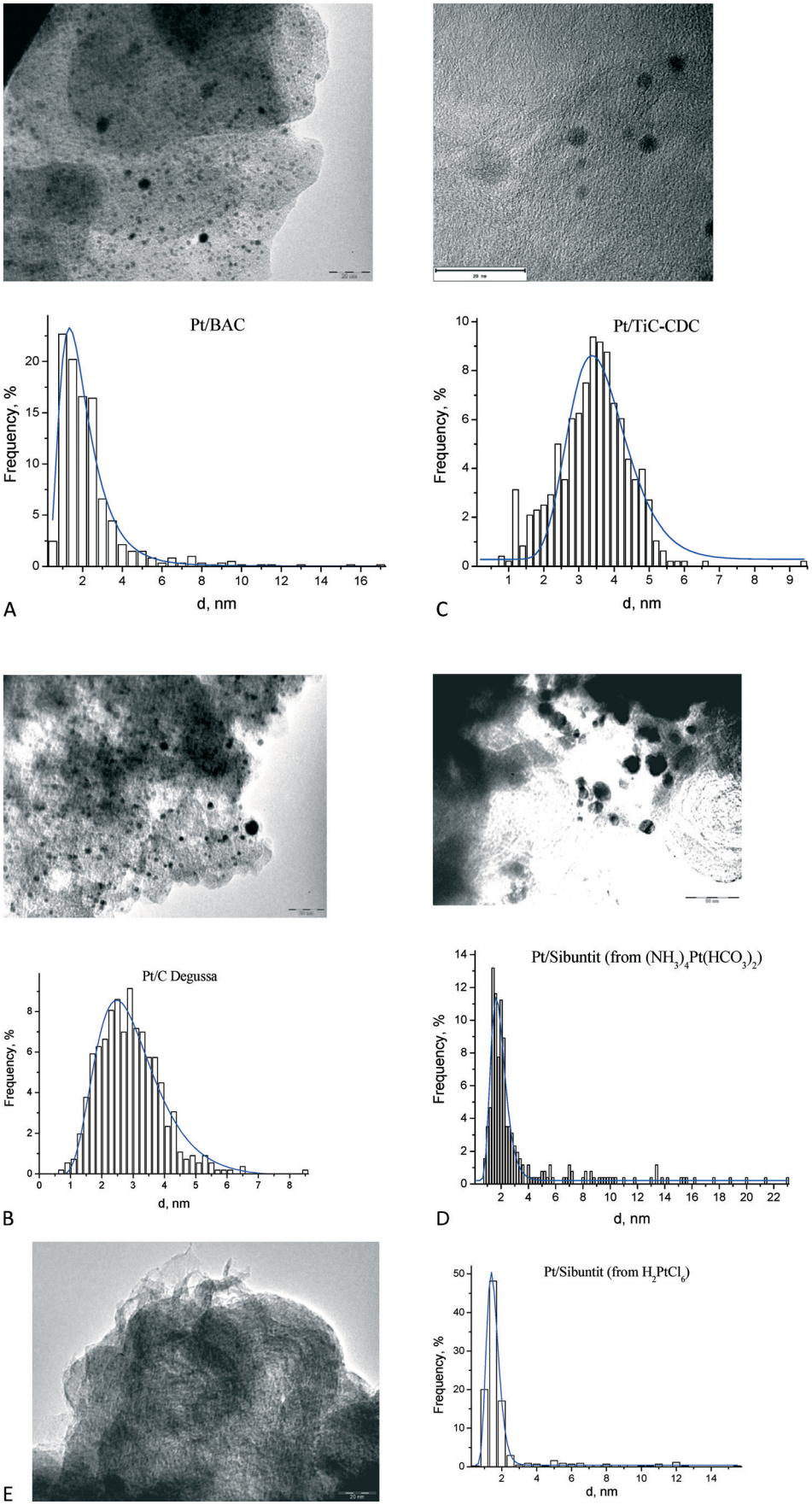

Fig. 1 TEM images and corresponding Pt particle size distribution for a) Pt/BAC, b) Pt/C (Degussa), c) Pt/TiC-CDC, d) Pt/Sibunit (I); e) Pt/Sibunit (II).

Table 2 Information on average Pt cluster sizes obtained from CO chemisorption and TEM

Catalyst	Pt content, wt.%	d_{Pt}, nm (CO chem.)	d_{Pt}, nm (TEM)
Pt/TiC-CDC	2.8	9.0	3.3 ± 1.0
Pt/C (Degussa)	5	2.4	2.8 ± 1.0
Pt/Sibunit (I)	5	9.0	3.4 ± 0.6
Pt/Sibunit (II)	5	2.8	1.9 ± 2.1
Pt/BAC	5	1.5	2.0 ± 1.8

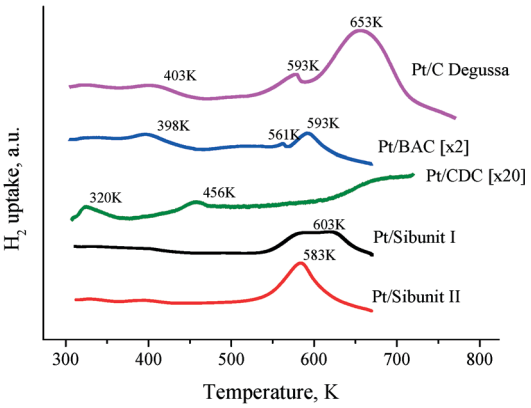

Fig. 2 Temperature-programmed reduction profiles for Pt/C catalysts.

differences in the surface acidity of the samples. Generally speaking, the surface acidity of carbon materials is determined by the surface chemistry of the carbons, *i.e.* by the functional groups presenting on the carbon surface[72] (*e.g.* carboxyl, carbonyl and hydroxyl species). Moreover, higher oxidation temperatures or a stronger oxidation agent result in more oxidized carbon materials.[73] Compared to other Pt/C catalysts Pt/TiC-CDC demonstrated the lowest value of the heat of desorption – 45 kJ mol^{-1}. The E_{des} calculated for Pt/Sibunit (II), prepared from hexachloroplatinic acid as a Pt source (54 kJ mol^{-1}), was almost the same as for Pt/Sibunit (I) (53 kJ mol^{-1}) prepared from the hydroxocarbonate Pt complex. The E_{des} values calculated for Pt/C (Degussa) and for Pt/BAC were somewhat lower – 51 kJ mol^{-1}. The total number of acid sites calculated as the amount of ammonia desorbed is shown in Table 3. The total acidity of the Pt/C catalysts decreases in the following order: Pt/BAC > Pt/Sibunit(II) > Pt/Sibunit(I) > Pt/C(Degussa) > Pt/TiC-CDC.

Thus, the Pt/TiC-CDC sample possessing the lowest value of E_{des} has also the lowest acidity. On the other hand, Pt/BAC containing the highest number of surface acid sites exhibited E_{des} of 51 kJ mol^{-1}, the same as that of Pt/C (Degussa). The fact, that some catalytic materials exhibiting higher values of E_{des} possess a lesser number of acid sites can be explained by the difference in the nature of the carbon material, Pt source and catalyst preparation technique.

Catalytic performance of the Pt/C in APR of xylitol

Catalyst stability studies. APR of xylitol solution was investigated over the five Pt/C catalysts at 498 K and 29.3 bar.

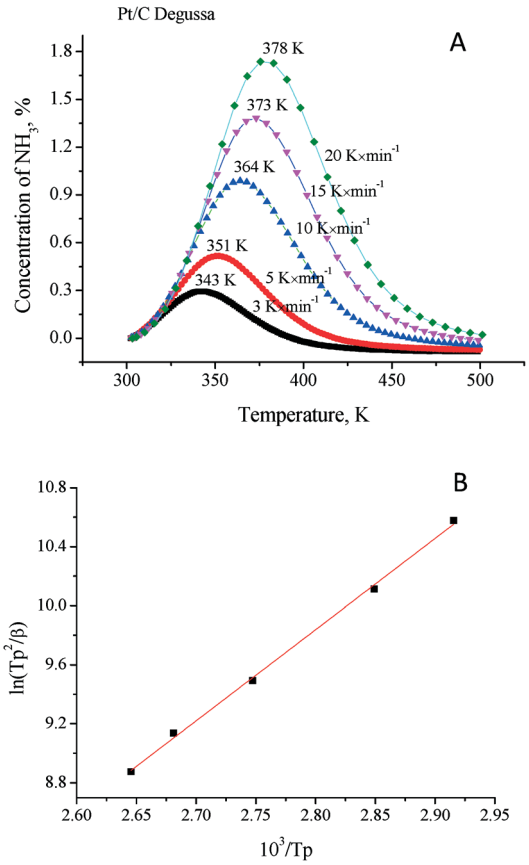

Fig. 3 NH_3-TPD curves registered for Pt/C Degussa (a) and determination of E_{des} (b).

Table 3 Acidic properties of Pt/C catalysts

Catalyst	Pt content, wt.%	Acidity, μmol g^{-1}	E_{des}, kJ mol^{-1}
Pt/TiC-CDC	2.8	6	45
Pt/C (Degussa)	5	47	51
Pt/Sibunit (I)	5	103	53
Pt/Sibunit (II)	5	92	54
Pt/BAC	5	158	51
Pt/Al_2O_3	5	317	52

Xylitol reforming comprises destruction of the initial molecule into H_2 and CO. The carbon monoxide formed further reacts with water *via* water–gas shift reaction to form CO_2 and additional H_2. The APR of xylitol can be therefore envisioned as a reaction of one mole of xylitol with five moles of water resulting in formation of eleven moles of H_2 and five moles of CO_2 as shown in Scheme 1.

On top of that, the hydrogen formed can participate in reactions with the initial polyol resulting in formation of alkanes as well as other products.[25,31] Therefore, the key parameters to study when comparing the catalytic performance of different catalysts are: conversion of xylitol, ability of converting carbon into gas phase products, selectivity to hydrogen (H_2/CO_2 ratio), and hydrocarbon selectivity.

An important issue to be addressed in APR is the catalyst stability. There are several factors causing catalyst deactivation

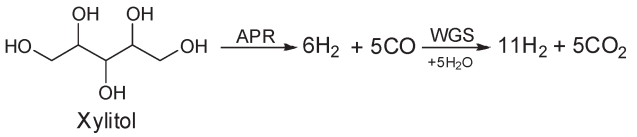

Scheme 1 APR of xylitol representing the stoichiometry of H_2 and CO_2 formed.

in APR:[74] low hydrothermal stability of the support,[52] leaching of the supported metal and formation of coke are among them.

The catalysts were studied for stability performance for at least 13 h time-on-stream (TOS). Pt/TiC-CDC was studied for more than 120 h of TOS. All catalysts showed minor or negligible deactivation with time-on-stream. The results are summarized in Table 4. For instance, conversion of xylitol over Pt/TiC-CDC changed from 58 to 47% and selectivity to H_2 from 77 to 71% after 120 h TOS in the APR at 498 K, 29.3 bar and WHSV = 1.2 h^{-1}. For other Pt/C catalysts a similar trend was observed, however, the changes in xylitol conversion and selectivity to H_2 did not exceed 10% compared to the initial values observed at 4 h TOS.

Profile of xylitol conversion and H_2/CO_2 ratio. The formation rates of the main APR products – H_2 and CO_2 – over Pt/TiC-CDC are shown in Fig. 4. It is important to note that with the decrease of conversion at higher space velocities the H_2/CO_2 ratio increases. Therefore, the higher space velocities are more favorable for selective production of hydrogen because of less hydrogen consumption. As can be seen from Fig. 5 displaying the xylitol conversion profile in the APR process over Pt/TiC-CDC, the conversion of xylitol decreases from 58% at 1.2 h^{-1} to 22% at 3.0 h^{-1} and then further to 11% at 3.6 h^{-1}. The H_2/CO_2 ratio indicating the selectivity to hydrogen increases as conversion of xylitol decreases as displayed in Fig. 5. At 58% conversion the calculated H_2/CO_2 ratio was 2 (being close to stoichiometric 2.2 as in Scheme 1); however, at 11% conversion it increases significantly to *ca.* 3.

Comparison of different Pt/C catalysts in the APR of xylitol. Catalysts exhibited a different ability of converting xylitol under the same experimental conditions (498 K, 29.3 bar, 3.0 h^{-1}) and the results are collected in Fig. 6.

The highest conversion of xylitol was achieved in the case of Pt/Sibunit (I) (32%). Pt/TiC-CDC was able to convert 22% of xylitol, whereas the xylitol conversion for Pt/BAC and Pt/Sibunit (II) was 22 and 15%, respectively. The Pt/C (Degussa) demonstrated the lowest value of the xylitol conversion among the Pt/C catalysts investigated – 8%. Thus, the catalysts can be ranked in the following order on the basis of xylitol conversion: Pt/Sibunit(I) > Pt/TiC-CDC > Pt/BAC > Pt/Sibunit(II) > Pt/C (Degussa).

Table 4 Time-on-stream behavior of Pt/C catalysts in the APR of xylitol

Catalyst	TOS, h	Xylitol conversion, %	Selectivity to H_2, %
Pt/TiC-CDC	10	58	77
	120	47	71
Pt/C (Degussa)	4	57	67
	16	55	67
Pt/Sibunit (I)	4	73	63
	13	72	62
Pt/Sibunit (II)	4	57	62
	16	53	61
Pt/BAC	4	76	60
	16	74	58

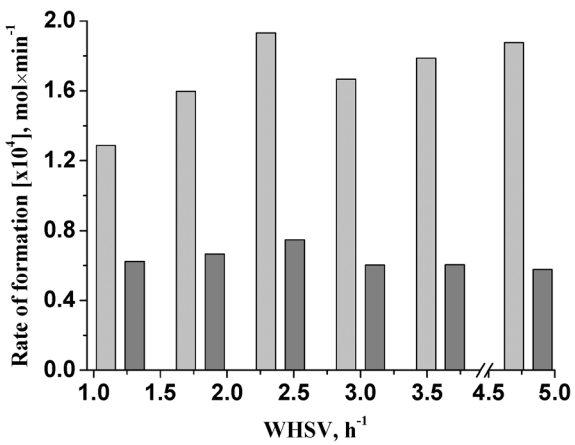

Fig. 4 Rate of H_2 (light grey columns) and CO_2 (dark grey columns) formation in the APR of xylitol over Pt/TiC-CDC. Conditions: 0.5 g of catalyst, 498 K, 29.3 bar, N_2 flow 30 ml min^{-1}, 10 wt.% xylitol solution.

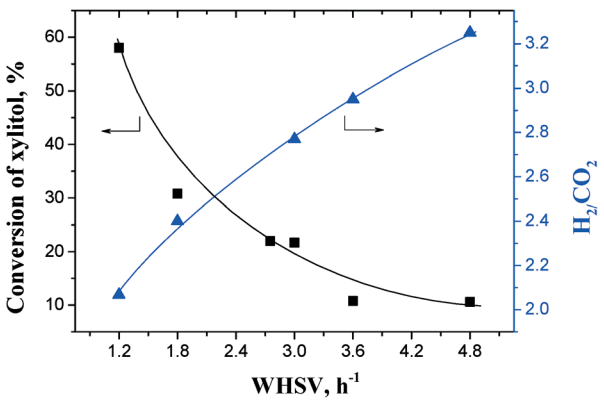

Fig. 5 Conversion of xylitol (■) and H2/CO2 (▲) ratio in the APR process over the Pt/TiC-CDC catalyst. Conditions: 0.5 g of catalyst, 498 K, 29.3 bar, N_2 flow 30 ml min^{-1}, 10 wt.% xylitol solution.

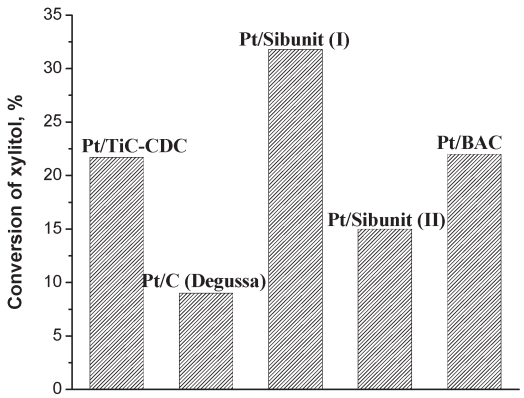

Fig. 6 Conversion of xylitol over different Pt/C catalysts in APR. Conditions: 498 K, 29.3 bar, N_2 flow 30 ml min^{-1}, 3.0 h^{-1}.

The conversion of the substrate in APR does not represent a transformation *per se* into the target products, since transformation of the initial feed may occur *via* several pathways, including dehydrogenation and dehydration steps as has been shown earlier for glycerol,[17] xylitol[25] and sorbitol[75] (Scheme 2, on the basis of results reported earlier[20,25]). The ratio H_2/CO_2 is of high significance in the APR process displaying the potential of Pt/C catalysts to selectively produce hydrogen. Moreover, as has been mentioned above, the hydrogen formation is accompanied with production of CO_2 in the APR process. The corresponding H_2/CO_2 ratios at xylitol conversions *ca.* 10–12% are shown in Fig. 7. All catalysts showed a H_2/CO_2 ratio above 2.2 with Pt/TiC-CDC being the most selective (H_2/CO_2 = 2.95 at 10% conversion). Slightly less selective behavior in terms of hydrogen production was observed for Pt/C (Degussa) (2.65) and Pt/Sibunit (II) (2.53) samples. The H_2/CO_2 ratio for Pt/BAC and Pt/Sibunit (I) was 2.37 and 2.30, respectively. The H_2/CO_2 ratios observed for Pt/C are above the theoretical ratio calculated from the polyol reforming equation as represented in Scheme 2 for xylitol. APR of polyol does not comprise only the reforming reaction proceeding *via* the pathway illustrated in Scheme 1. In fact, the reaction is more complex[25] and includes several transformations of the substrate resulting in the elimination of H_2 and CO, which are further transformed into CO_2 and H_2O *via* WGS reaction and formation of oxygenates (Scheme 2). Since APR reaction is not limited to the formation of H_2 and CO_2, the H_2/CO_2 ratio might differ from the theoretical one. In the case when a part of carbon is not converted into CO_2, the H_2/CO_2 ratio will be higher than the theoretical one based on the reaction equation shown in Scheme 1.

An important parameter in the APR process of polyols is the ability of a catalyst to convert carbon into gas phase products, in other words, to cleave C–C bonds in the substrate.

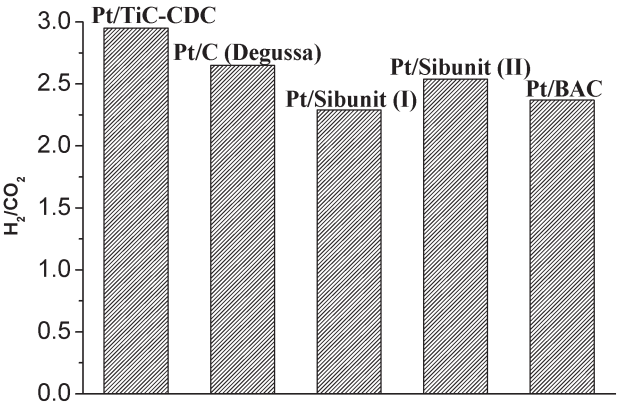

Fig. 7 H_2/CO_2 ratio for different Pt/C catalysts in APR of xylitol. Conditions: 0.5 g of catalyst, 498 K, 29.3 bar, N_2 flow 30 ml min^{-1}, 10 wt.% xylitol solution, conversion ~ 10–12%.

The conversion of carbon to gaseous products in APR of xylitol is shown in Fig. 8. As can be noted, the most active catalyst is Pt/C (Degussa) with 13.6% of carbon converted into the gaseous products at 10% of xylitol conversion. The Pt/BAC catalyst was able to convert 10.5% of carbon, whereas the corresponding values found for Pt/TiC-CDC, Pt/Sibunit (II) and Pt/Sibunit (I) were 8.5%, 5.6% and 4.4%, respectively.

The following order on the basis of carbon converted into the gas phase can be presented: Pt/C(Degussa) > Pt/BAC > Pt/TiC-CDC > Pt/Sibunit(II) > Pt/Sibunit (I).

During APR of xylitol the formation of alkanes C_1–C_5 takes place as a result of dehydration and further hydrogenation reactions.[20] Hydrocarbon formation *versus* WHSV in the APR of xylitol over the Pt/TiC-CDC catalyst is presented in Fig. 9. In general, all the catalysts have similar compositions of the hydrocarbon mixtures formed with C_1–C_3 dominating in the mixture. Butane was found in minor quantities as well as CO.

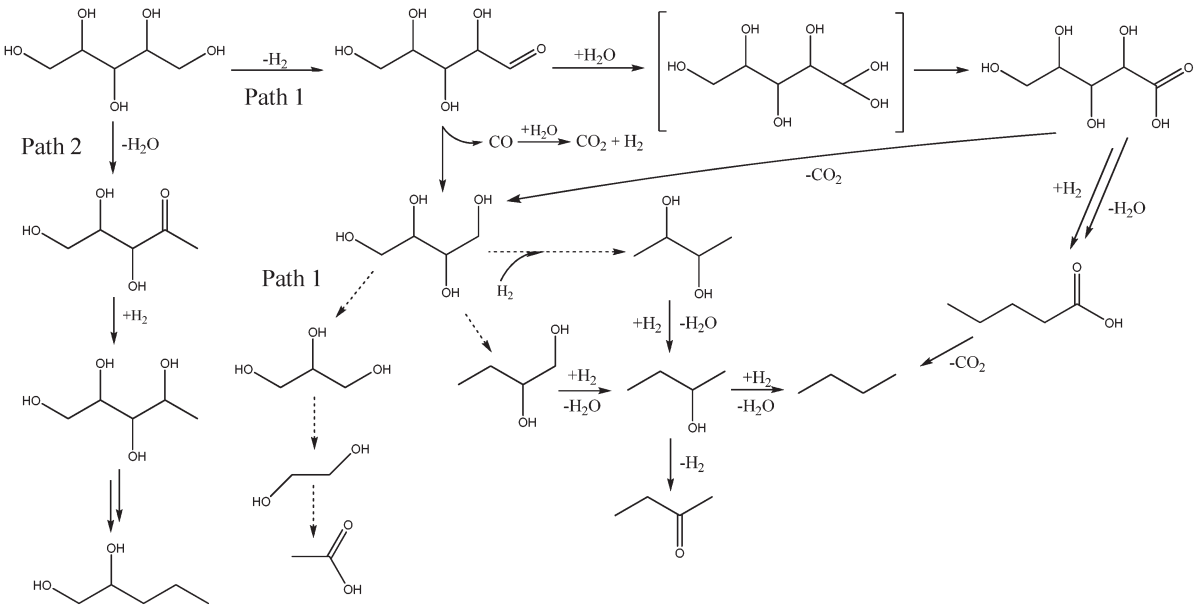

Scheme 2 APR of xylitol: the main transformation pathways.

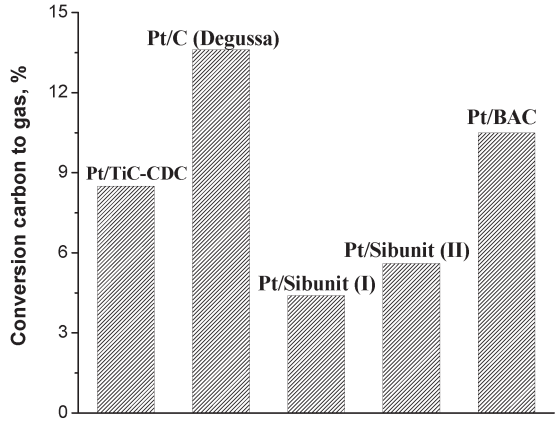

Fig. 8 Conversion of carbon to gas phase products for different Pt/C catalysts in APR of xylitol. Conditions: 0.5 g of catalyst, 498 K, 29.3 bar, N_2 flow 30 ml min^{-1}, 10 wt.% xylitol solution, conversion ~ 10–12%.

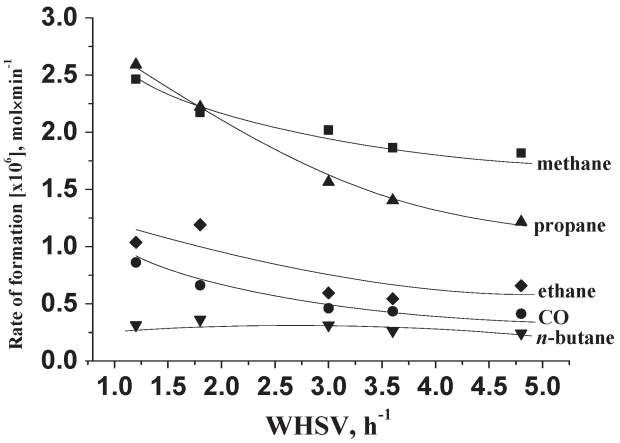

Fig. 9 Composition of hydrocarbons mixture in the APR of xylitol over Pt/TiC-CDC. Conditions: 0.5 g of catalyst, 498 K, 29.3 bar, N_2 flow 30 ml min^{-1}, 10 wt.% xylitol solution.

The formation rates of all hydrocarbons as well as carbon monoxide demonstrated a decreasing trend with an increase in WHSV or in other words in a decrease of conversion. Pentane concentration for all the experiments was below the detection limit. It might be the case that pentane is not formed since significantly higher surface acidity than those possessed by the used carbon-supported catalysts is required.[26,76]

A comparative analysis of Pt/C catalysts in terms of hydrocarbon formation is shown in Fig. 10. The hydrocarbon formation rate in the case of Pt/BAC was more than 1.5 times higher compared to both Pt/Sibunit samples and twofold higher compared to Pt/C (Degussa). The lowest rate of hydrocarbon formation was observed in the case of Pt/TiC-CDC being almost four times lower in rate than that of Pt/BAC.

The catalytic data obtained for the Pt/C catalysts are summarized in Table 5. As can be seen, for all the catalysts with an increase in WHSV, the conversion of xylitol decreases. Meanwhile the H_2/CO_2 ratio is higher at lower conversion of the initial substrate, meaning less consumption of hydrogen therefore the H_2/CO_2 ratio increases with a decrease in the

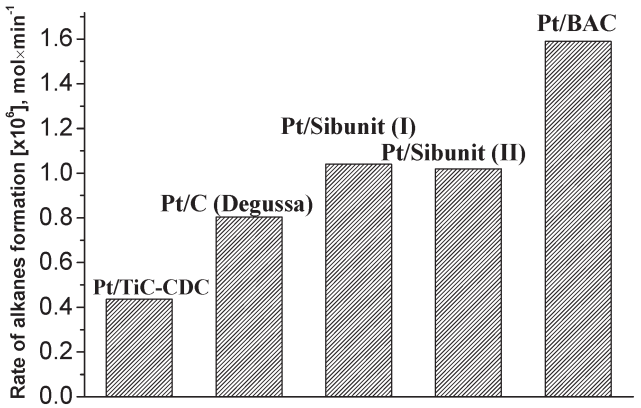

Fig. 10 Rate of hydrocarbon formation for different Pt/C catalysts in APR of xylitol. Conditions: 0.5 g of catalyst, 498 K, 29.3 bar, N_2 flow 30 ml min^{-1}, 10 wt.% xylitol solution, conversion ~ 10–12%.

xylitol conversion. The results indicating an increase of hydrogen-to-carbon dioxide ratio at lower conversions in APR over Pt/C are in line with the data previously reported for Pt/Al_2O_3.[25] Opposite to the H_2/CO_2 ratio, the selectivity to alkanes is lower at higher space velocities for all the catalysts studied. Since hydrogen formation is competing with hydrocarbon formation in APR[32] the trend of hydrocarbon selectivity to increase with a decrease of hydrogen selectivity is understandable.

Correlation between catalyst structure and catalytic performance in APR of xylitol over Pt/C. All Pt/C catalysts demonstrated a different behavior in the APR of xylitol in terms of substrate conversion and selectivity towards the main products such as H_2 and CO_2 as well as hydrocarbons. The main reasons for determining catalytic behavior are the textural and surface properties of the catalytic materials.

Based on CO chemisorption data (Table 1), corresponding TOF values for Pt/C catalysts studied in the present work were calculated. As a result a dependence of TOF for hydrogen production on average Pt cluster size is displayed in Fig. 11. The TOF increases linearly with an increase in the average size of the Pt cluster in the APR of xylitol thus indicating that APR of xylitol is a structure-sensitive reaction. Lehnert and Claus, explaining the increase in the hydrogen formation rates during APR of glycerol over Pt/Al_2O_3 catalysts with different dispersions, proposed that adsorption and C–C cleavage of polyol species preferably occurred on the face Pt atoms rather than on edge and corner atoms. With an increase in the cluster size the number of face atoms increases whereas the number of corner and edge atoms should decline.[77] The volume of Pt clusters is proportional to r^3, while the surface area, to r^2, where r is a radius of Pt particles. Therefore, assuming that face Pt atoms are much active in APR than edge and corner atoms, the catalytic activity, *i.e.* TOF should increase linearly with an increase of the average size of the Pt cluster. However, at a certain size of the Pt cluster the role of corners and edges can be neglected and TOF reaches a plateau. The results regarding the TOF dependence on the average size of Pt clusters in xylitol APR are in very good

Table 5 Catalytic data for APR of xylitol over Pt/C at different weight hour space velocities[a]

	Pt/TiC-CDC			Pt/C Degussa			Pt/Sibunit (I)			Pt/Sibunit (II)			Pt/BAC			Pt/Al_2O_3		
WHSV, h^{-1}	1.2	3.0	4.8	1.2	3.0	4.8	1.2	3.0	4.8	1.2	3.0	4.8	1.2	3.0	4.8	1.2	3.0	4.8
Conversion, %	56	12	11	57	9	3	73	32	1	57	15	13	76	22	15	82	43	27
C_{gas}, %	23.3	8.5	5.0	38.5	13.6	7.1	31.9	14.0	7.4	32.6	12.4	5.6	49.0	15.9	10.5	39.1	16.6	8.8
H_2/CO_2	2.0	2.8	3.0	2.2	2.7	2.9	1.9	2.3	2.6	1.8	2.4	2.5	1.8	2.0	2.4	2.5	2.7	2.9
S_{alk}, %	19	14	1	15	12	11	21	17	14	22	17	14	22	19	19	4.6	4.9	4.2

[a] Conditions: 0.5 g of catalyst, 498 K, 29.3 bar, 10 wt.% xylitol solution, 30 ml min^{-1} N_2 flow rate.

agreement with the results reported earlier for APR of glycerol and ethylene glycol.

Another important catalyst characteristic bearing a significant effect on the catalytic performance is the acidity of the catalytic material. Generally, it is assumed that more acidic supports facilitate the formation of hydrocarbons in APR since the key step in alkane formation is dehydration of polyol[32] (Scheme 2). It has been shown recently that acidic and basic properties of the support play a key role in hydrogen formation in APR of glycerol.[78] On top of that, the addition of Re increases the acidity of Pt/C catalysts thus resulting in elevated formation of alkanes from glycerol as demonstrated by Zhang *et al.*[43] Fig. 12 shows a clear correlation between the acidic properties of the Pt/C catalysts elucidated by NH_3-TPD and catalytic performance in the APR of xylitol. As can be seen from Fig. 12, with an increase in the total acidity of the catalysts the selectivity to H_2 decreases, while the rate of hydrocarbon production increases, illustrating that formation of hydrogen and hydrocarbons are competing reactions during APR. Thus, when more hydrogen is formed less hydrocarbons can be produced. Zhang *et al.*[43] demonstrated that the ability of the catalyst to cleave C–O bonds (responsible for hydrocarbons formation) is enhanced when more Re is added to Pt (thus increasing the total acidity of the catalytic material). Besides, Criftci *et al.*[78] demonstrated that less acidic supports are more favorable for selective production of hydrogen. Additionally, higher selectivities to hydrogen were observed in APR of glycerol when using such basic supports for Pt as $Mg(Al)O_x$.[79] Therefore, the correlation

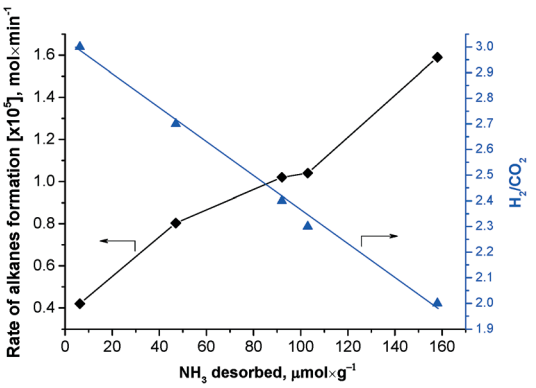

Fig. 12 Dependence of alkanes formation rate and H_2/CO_2 ratio on a surface acidity of Pt/C catalysts. Conditions: 498 K, 29.3 bar, N_2 flow 30 ml min^{-1}, conversion ~10–12%.

between the acidity of the catalytic materials investigated in the present study is in a perfect correspondence with data reported previously in the literature regarding APR of glycerol.

APR of xylitol over carbon- and metal oxide supported Pt catalysts: effect of the support. In order to reveal the influence of the support on the catalytic activity and selectivity towards the main products a comparison of Pt/C and Pt/MO_x catalysts in the APR of xylitol under identical experimental conditions was performed. The data are collected in Table 6. For comparison three carbon supported catalysts, Pt/TiC-CDC, Pt/C (Degussa) and Pt/Sibunit (II) were selected. As for metal oxide supported Pt catalysts, Pt/Al_2O_3 (Degussa) was chosen. As can be seen from Table 6, Pt/C (Degussa) demonstrated the highest conversion of carbon to gas phase products. Carbon supported catalysts displayed in general higher conversion of carbon into gas phase products at the same xylitol conversion level than Pt supported on Al_2O_3. A similar trend was observed by Kim *et al.*[51] for APR of glycerol over Pt–Re catalysts supported on carbonaceous materials CMK-3, oxide supports as well as SiO_2 at 523 K, 45 bar and 2.0 h^{-1}. The order on the basis of carbon conversion into gas phase products is the following: Pt/C (Degussa) > Pt/Sibunit (II) > Pt TiC-CDC > Pt/Al_2O_3. Shabaker *et al.*[4] reported higher carbon turnover frequencies in APR of ethylene glycol: the total carbon TOF (comprising CH_4, CO_2 and C_2H_6) in the case of Pt/C was 4.88 min^{-1} whereas it was 3.07 min^{-1} for Pt/Al_2O_3. The H_2/CO_2 ratio for the catalysts studied decreases in the following order: Pt/Al_2O_3 > Pt/C (Degussa) > Pt/TiC-CDC > Pt/Sibunit (II).

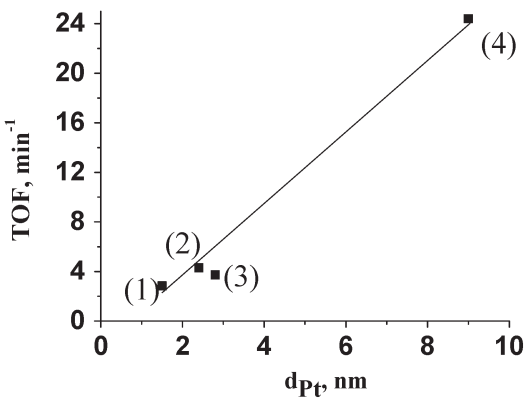

Fig. 11 Dependence of TOF *versus* mean Pt cluster size in APR of xylitol. Conditions: 498 K, 29.3 bar, N_2 flow 30 ml min^{-1}, conversion ~10–12%. (I) – Pt/BAC, (II) – Pt/C (Degussa), (3) – Pt/Sibunit (II), (4) – Pt/TiC-CDC.

Table 6 Comparison between Pt/C catalysts and Pt/Al_2O_3 in the APR of xylitol[a]

Catalyst	Pt content, wt.%	D,[b] %	Carbon to gas, %	H_2/CO_2	S_{alk}, %	TOF_{H2}, min^{-1}	TOF_{alk}, min^{-1}
Pt/TiC-CDC	2.8	12	23.3	2.0	19	16.7	0.80
Pt/C (Degussa)	5	47	38.5	2.2	15	4.0	0.16
Pt/Sibunit(II)	5	41	32.6	1.8	22	3.0	0.24
Pt/Al_2O_3	5	29	21.1	2.5	4.6	8.5	0.10

[a] Conditions: 0.5 g of catalyst, 498 K, 29.3 bar, 10 wt.% xylitol solution, 30 ml min^{-1} nitrogen flow rate, conversion of xylitol ~55–57%. [b] Calculated based on CO chemisorption.

Likewise, Kim *et al.* observed the difference in the selectivity to hydrogen for Pt–Re supported catalysts in APR of glycerol.[51] Pt–Re supported on alumina was the most selective (77%) catalyst; the SiO_2-supported catalyst demonstrated a comparable selectivity to the CMK-3-supported material being 61.7 and 61.6%, respectively. The lowest selectivity to H_2 was observed in the case of Pt–Re/AC which exhibited an S_{H2} of only 57.1%.

Since production of hydrogen competes with formation of hydrocarbons in APR, the catalysts which demonstrated the lowest H_2/CO_2 values possessed the highest selectivity to alkanes. Thus, the selectivity to alkanes decreases in the following order: Pt/Sibunit (II) > Pt/TiC-CDC > Pt/C (Degussa) > Pt/Al_2O_3.

The results are in good correlation with the previous work on APR of glycerol:[51] selectivity to alkanes decreased in the following order: Pt–Re/AC > Pt–Re/CMK-3 > Pt–$ReSiO_2$ > Pt–Re/Al_2O_3.

Based on the data obtained from CO chemisorption, the corresponding values of turnover frequencies of hydrogen and alkane formation can be calculated (Table 6). The highest value of TOF_{H2} was observed in the case of Pt/TiC-CDC catalyst being equal to 16.7 min^{-1}. Compared to Pt/TiC-CDC, Pt/Al_2O_3 demonstrated an almost twofold lower value of TOF_{H2}, 8.5 min^{-1}. The TOF values of H_2 generation for Pt/C (Degussa) and Pt/Sibunit (II) were 4.0 and 3.0 min^{-1}, respectively. It is worth mentioning that Pt supported on carbon turned out to be more catalytically active also in hydrocarbon production *via* APR than Pt/Al_2O_3 as evidenced by the corresponding TOF_{alk} values presented in Table 6. Thus the TOF_{alk} values in APR of xylitol decrease in the following order: Pt/TiC-CDC > Pt/Sibunit (II) > Pt/C (Degussa) > Pt/Al_2O_3.

The supported Pt–Re catalysts studied by Kim *et al.*[51] were placed in the following order based on the volumetric hydrogen production rates: Pt–Re/CMK-3 > Pt–Re/AC > Pt–Re/SiO_2 > Pt–Re/Al_2O_3. The authors noticed that carbon supports (both CMK-3 and AC) showed a better performance in terms of hydrogen production than alumina and silica supported catalysts. After calculating TOF_{H2} based on the values of hydrogen production rates and metal dispersion, the following order can be presented: Pt–Re/AC > Pt–Re/SiO_2 ~ Pt–Re/CMK-3 > Pt–Re/Al_2O_3.

This order clearly shows the effect of support on hydrogen production *via* APR of glycerol (TOF_{H2} values were calculated using literature data and the equation described in the Experimental section).

Increased hydrogen production affected by the type of support was also shown[50] for bimetallic Pt–Mn catalysts in APR of ethylene glycol. It has been demonstrated that the conversion of ethylene glycol decreased in the following order: Pt–Mn/CMK-3 > Pt–Mn/AC > Pt–Mn/Al_2O_3. The proposed reason for superior behavior of Pt–Mn/CMK-3 in terms of hydrogen production was connected to the ordered pores and opened mesopores of the CMK-3 support structure. The latter one provides easier access of the reactants and facilitates desorption of the products, *i.e.* (H_2, CO_2, alkanes) from the catalytic material without diffusion resistance.[80]

Shabaker *et al.*[4] reported efficient catalytic performance of carbon supported catalysts over Pt/Al_2O_3 in the APR of ethylene glycol in terms of hydrogen and hydrocarbons production. The TOF_{H2} values for Pt/C were slightly higher than those observed for Pt/Al_2O_3 in APR of EG. It is important to note that the TOF_{alk} values were also higher in the case of Pt/C than for Pt/Al_2O_3.

The superior catalytic behavior of Pt/C catalysts, especially Pt/TiC-CDC, compared to the alumina supported sample, can be linked to the higher surface area of the carbon supported materials and enhanced hydrothermal stability under severe APR conditions. Similar to the case of CMK-3 based catalysts,[50,51] the narrow pore size distribution inside carbide-derived carbons as well as regular structure and high surface area of carbons might facilitate APR thus resulting in enhanced TOF_{H2} and TOF_{alk}. Furthermore, the interactions between Pt and carbide-derived support might enhance the catalytic performance.[70]

Conclusions

The APR of xylitol was investigated over five different carbon supported Pt catalysts: Pt/TiC-CDC, Pt/C (Degussa), Pt/Sibunit (I and II) and Pt/BAC.

The catalysts demonstrated minor deactivation with time-on-stream. The decrease in xylitol conversion after 120 h of catalytic performance for Pt/TiC-CDC did not exceed 10%.

The catalysts possess different textural and acid–base properties. Therefore, it was possible to study the effect of surface acidity on the formation of hydrogen and alkanes. For the first time the structure sensitivity in APR of polyols containing more than three carbon atoms was found and studied. The TOF linearly depends on the average size of the Pt cluster and increases with an increase in the cluster size within the studied cluster size domain. The results obtained are in very good correlation with previously reported data on

APR of ethylene glycol and glycerol. A plausible explanation for the TOF increase with an increase in Pt cluster size was proposed. The highest TOF values in terms of hydrogen production were observed for Pt supported on carbide-derived carbon. This material has shown a high potential in the APR of xylitol since the Pt/TiC-CDC catalyst exhibited both selective (H_2/CO_2 ~ 3) and effective production of hydrogen. The TOF_{H2} values observed in the case of Pt/TiC-CDC were twofold higher compared to those of Pt on alumina and more than four times higher compared to those of platinum on activated carbon and Sibunit. Moreover, the TOF for alkane formation in the case of Pt/TiC-CDC was 0.80 min^{-1} which is eight times more compared to that of Pt/Al_2O_3.

The results obtained from NH_3-TPD studies revealed a correlation between Pt/C acidity and catalytic performance. It was found that catalytic materials bearing high acidity favor the formation of hydrocarbons. On the contrary, Pt/C catalysts possessing low (Pt/C (Degussa) or very low (Pt/TiC-CDC) acidity were effective in hydrogen formation. Another important advantage of Sibunit and carbide-derived carbon supports is high mechanical stability. This in turn facilitates their use as catalytic supports in continuous fixed-bed reactors.

To conclude, carbon supports have great potential in APR, since they are available, stable under hydrothermal conditions and possess a variety of textural and surface properties, which can be tuned to obtain the desirable catalytic material. It has been shown that by the choice of carbon material, its nature, pretreatment of the carbon support, as well as by the choice of Pt source it is possible to steer the APR of polyols towards sustainable hydrogen or hydrocarbon production.

Experimental part

Catalyst preparation

All chemicals for catalyst synthesis (H_2PtCl_6, $Pt(NH_3)_4(HCO_3)_2$) (>99.9%) were purchased from commercial suppliers and used without further purification. Titanium carbide (TiC) was purchased from Goodfellow with a purity >99.8% and a mean particle size of 75 μm. The platinum precursor $[Pt(NH_3)_4]Cl_2$ was purchased from Alfa Aesar with a purity of 99.9%; 65 wt.% HNO_3 was purchased from AppliChem as pure acid.

5 wt.% Pt/Sibunit

Preparation of the Sibunit support. Sibunit was placed in a glass reactor for calcination and calcined in a flow of dry air (50 ml min^{-1}) using the following procedure: from 298 K to 373 K within 60 min, 373 → 433 K within 4 h, then 433 → 493 K within 4 h, 493 K → 553 K within 4 h, 553 K → 623 K within 4 h, then cooling 623 K → ambient temperature within 2 h. Calcined Sibunit was then crushed in a porcelain mortar and sieved. A fraction of 0.16–0.4 mm was collected.

Preparation of 5 wt.% Pt/Sibunit from H_2PtCl_6. A solution containing 0.546 g of H_2PtCl_6 in 14 ml of distilled water (total Pt content 0.26 g) was added to 5 g of Sibunit (fraction 0.16–0.4 mm). Then an additional amount of distilled water was added until the total volume of the slurry was 50 ml. The slurry formed was stirred for 2 h at 323 K. After impregnation the sample was dried at 398 K in air for 12 h. The catalyst was further calcined in air using the following temperature program: 298 K → 623 K within 24 h, dwell at 623 K for 2 h. The calcined sample was flushed with dry Ar and reduced in hydrogen using the following temperature ramp: 298 K → 573 K within 2 h and at 573 K for 1.5 h.

Preparation of 5 wt.% Pt/Sibunit from $Pt(NH_3)_4(HCO_3)_2$. A solution containing 0.85 g of the Pt precursor in 50 ml of distilled water was added to 8 g of Sibunit (fraction 0.16–0.4 mm). Distilled water was added until the total volume of the slurry reached 200 ml. The suspension obtained was stirred for 2 h at 323 K. The sample was dried, calcined and reduced following the same procedure as described above for Pt/Sibunit (from H_2PtCl_6).

5 wt.% Pt/BAC

The solution of $Pt(NH_3)_4(HCO_3)_2$ containing 0.85 g of the complex in 50 ml of distilled water was added to the activated carbon (from birch, 8 g). The platinum salt was added in dissolved form. While monitoring the pH (acidic), the solution was neutralized by sodium carbonate for formation of hydroxides precipitated on the support, which were then readily reduced. The catalyst was reduced chemically using formic acid. Sodium acetate, which prevents peptisation (coagulation) of the metal according to,[81] and the reducing agent formic acid were added dropwise under stirring at 363 K. After stirring the mixture for 1 h, the solution was cooled down and a sample was withdrawn for a qualitative analysis to confirm that there were no chloride ions present in the solution after the impregnation.

2.5 wt.% Pt/TiC-CDC (carbide-derived carbon)

Preparation of the TiC-CDC support. Titanium carbide (TiC, fraction 50–150 μm) was used as a precursor for the preparation of the TiC-CDC support. Hereby the carbide was subjected to chlorination in an alumina tubular reactor at 1473 K (C_{Cl2} = 1.5 mol m^{-3}, reactor diameter 3.2 cm, flow rate of 3 cm s^{-1}) using a mixture of Cl_2 and Ar. After a chlorination time of typically 5 h, 5 g of carbide was converted into 1 g of TiC-CDC. The material obtained was then treated with hydrogen for at least 30 min at the chlorination temperature to remove residual chlorine and metal chlorides from the pores of the carbon support and terminate its surface with hydrogen.

The obtained carbon support was treated with 65 wt.% HNO_3 at 363 K for 2 h using 50 ml acid per 1 g TiC-CDC. The carbon support obtained was filtered, washed with large amount of distilled water until pH 7 and dried at 353 K in air.[64,82]

Preparation of 2.5 wt.% Pt/TiC-CDC. Impregnation was performed with an ion adsorption method where the volume of impregnation solution containing the catalyst precursor material exceeds the pore volume of carbon material. The

charged precursor is bound and stabilized at the surface *via* Coulomb forces[83–85] at a distinct pH below or above the point of zero charge (PZC) of the support. Hereby the ratio of impregnation solution to carbon was adjusted to 50 $ml_{solution}\ g_{TiC\text{-}CDC}^{-1}$. The desired loading of platinum on carbon was 2.5 wt.%. As the precursor material $[Pt(NH_3)_4]Cl_2$ was dissolved in water leading to a cationic precursor complex, the pH of the solution was adjusted to pH 3.5 using HNO_3. After an addition of acid functionalized TiC-CDC the pH of the suspension was controlled and readjusted with NaOH or HNO_3 if necessary. The suspensions were stirred at room temperature for 24 h and subsequently filtered. The impregnated TiC-CDC filter cake was then washed with 200 ml of an HNO_3 dilution of equal pH as the impregnation solution and subsequently dried in an oven at 353 K overnight. In the last step, the catalyst precursor on the impregnated TiC-CDC was reduced at 673 K with 12 $L_N\ h^{-1}$ of 20 vol.% H_2 in N_2 in a tubular reactor.[64,82] The real Pt content determined by ICP-OES was 2.8% thus the subsequent designation (2.8%) was used for Pt/TiC-CDC.

5 wt.% Pt/C (Degussa)

The commercial catalyst 5 wt.% Pt/C (F 1525 XKT/W) was delivered by Degussa and used as received. The catalyst contains 5 wt.% of Pt according to the specification.

5 wt.% Pt/Al_2O_3

The Pt/Al_2O_3 catalyst is a commercial catalyst provided by Degussa (F 214 XSP). The catalyst contains 5 wt.% of Pt according to the specification.

Catalyst characterization

Prior to characterization as well as catalytic measurement all the catalysts were pre-dried overnight at 373 K in an oven in air to remove moisture.

The metal dispersion was determined by CO pulse chemisorption in an apparatus manufactured by Micromeritics (Autochem 2900). The catalyst was reduced prior to the measurement with the following program: 298–353 K at 10 K min^{-1} in He, dwell for 30 min, gas-switch to H_2, 5 K min^{-1} to 523 K, dwell for 2 h, followed by flushing for 60 min in He at 523 K to remove surface hydrogen. Thereafter the catalyst was cooled to ambient temperature and CO pulses were introduced utilizing 10 vol.% CO in He. For data evaluation a Pt/CO stoichiometry 2of 1 : 1 is assumed.

Transmission electron microscopy (TEM) measurements were performed with LEO 912 Omega, voltage 120 kV. The samples for TEM were prepared as a suspension of ethanol and for calculating the diameter of particles *ca.* 500 particles for each sample were taken.

The surface area and pore volume data for the Pt/C catalysts were obtained by low-temperature N_2 adsorption using Micromeritics ASAP 2010. For determination of the specific surface area the BET equation (Pt/TiC-CDC, Pt/Sibunit I and II) or the Dubinin equation for microporous carbons was applied (Pt/BAC, Pt/C (Degussa)).

The metal loading of all the catalysts (with the nominal wt% loadings given in the catalyst descriptor) was determined by ICP-OES using Perkin-Elmer Optima 4300.

The temperature-programmed reduction (TPR) (Micromeritics, Autochem 2910) was measured by placing approximately 0.1 g of Pt catalyst in a U-shaped tube, which was cooled to 298 K in argon. The catalyst was reduced using 5% H_2 in Ar with the temperature being ramped from 298 K to 723 K at a rate of 5 K min^{-1} and the hydrogen uptake monitored by a thermal conductivity detector (TCD).

The NH_3-TPD measurements were performed using Micromeritics Autochem 2910 apparatus. The procedure for determination of catalyst acidity by NH_3-TPD is similar to the one described by Souza and co-workers for Ni–Cu catalysts.[86] The same method was recently applied to acidity determination of Pt– and $PtRe/TiO_2$ catalysts.[87] Prior to NH_3 treatment the catalyst sample (0.1 g) was dried in an oven at 373 K overnight. The sample was then placed in a U-shape quartz tube and reduced under a hydrogen flow (20 ml min^{-1}) using the following procedure: 5 K min^{-1} to 523 K, dwell for 2 h. The catalyst was then flushed in a flow of He (20 ml min^{-1}) for 30 min to remove hydrogen from the catalyst surface. The sample was cooled down to ambient temperature and saturated with NH_3 (gas mixture 5% of NH_3 in He) for 1 h. Then, the gas mixture was switched back to He and the catalyst was flushed for 30 min to remove physically adsorbed ammonia. Temperature-programmed desorption was realized by heating up to 498 K at 3 K min^{-1}. Quantification of ammonia desorbed was done by monitoring changes of the calibrated TCD signal (calibrated with 5 vol.% of NH_3 in He). The number of acid sites was calculated through the measured amount of ammonia desorbed from a sample. For determination of the heat of desorption, after the first desorption of ammonia, a new saturation of a sample with ammonia was performed. The sample was treated by mixture of ammonia in helium as described above. The desorption was realized by heating to 498 K at various heating rates (5, 10, 15, 20 K min^{-1}). Heat of desorption was calculated using a standard approach which includes plotting T_p (temperature at maximum of desorption) *versus* $\ln(T_p^2/\beta)$ (where β corresponds to a heating rate) followed by calculation of the slope, and then E_{des} [kJ mol^{-1}].

Typical reaction procedure

For the APR studies reported in the present work, a continuous fixed-bed reactor setup (stainless steel reactor, d = 4.8 mm, l = 18 cm) equipped with a furnace was used. The reactor scheme is shown in Fig. 13. In the standard experiment the catalyst (0.5 g) was mixed with *ca.* 3 g of quartz sand and loaded to the reactor. The catalyst was reduced prior to the measurements with H_2 using the following program: 298 → 523 K at 5 K min^{-1} in hydrogen for 2 hours, at a hydrogen flow rate of 30 ml min^{-1}.

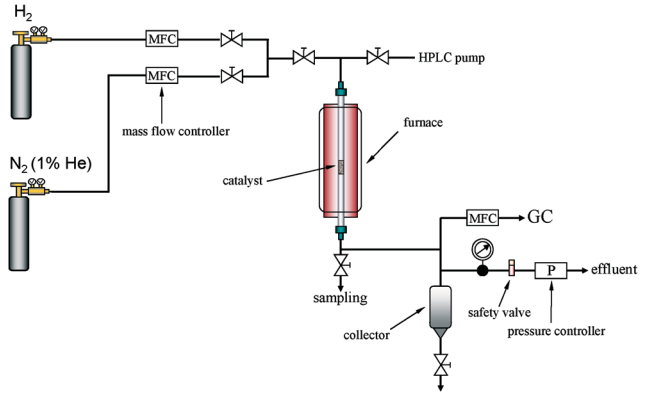

Fig. 13 Continuous fixed-bed reactor applied for APR of xylitol.

The reaction was carried out at 498 K and 29.3 bar, at a range of space velocities of 0.9–6.0 h^{-1}. The weight hour space velocity (WHSV) is defined as mass of substrate fed per mass of the catalyst per hour [g_{sub} g_{cat}^{-1} h^{-1}]. An aqueous solution (10 wt.%) of xylitol was used as the feedstock and fed in a continuous manner *via* an HPLC pump. Liquid samples were withdrawn periodically and analyzed by means of high-performance liquid chromatography (HPLC), applying an injection volume of 2 μl, Aminex HPX-87H column, eluent 5 mM H_2SO_4, flow rate 0.6 ml min^{-1}, 318 K, 70 min, applying a refractive index (RI) detector to determine conversion of xylitol.

The gaseous products were taken periodically and analyzed by means of a micro-GC (Agilent Micro GC 3000A). The instrument was equipped with 4 columns: Plot U, OV-1, Alumina and Molsieve. The micro-GC was calibrated to perform quantitative analysis for the following gases: H_2, CO_2, CO, CH_4, linear hydrocarbons C_1–C_4 and 1 wt.% of He in N_2 was used as an internal standard. Moreover, the carbon balance was monitored by means of total organic carbon analysis (TOC instrument) and was confirmed to a degree of 95–100% for all the measurements.

Calculation of the turnover frequency (TOF), selectivity to H_2 and alkanes

Turnover frequencies for Pt/C catalysts were calculated using the following equation:

$$\mathrm{TOF}_{\mathrm{H2}}\left[\mathrm{min}^{-1}\right] = \frac{r(\mathrm{H}_2)\left[\mathrm{mol\ min}^{-1}\right]}{\nu(\mathrm{M})[\mathrm{mol}]\cdot D[\mathrm{a.u.}]} \qquad (I)$$

where $r(H_2)$ denotes the rate of H_2 formation, ν(M) – moles of Pt and D – dispersion

$$\mathrm{TOF}_{\mathrm{alk}}\left[\mathrm{min}^{-1}\right] = \frac{r(\mathrm{alk})\left[\mathrm{mol\ min}^{-1}\right]}{\nu(\mathrm{M})[\mathrm{mol}]\cdot D[\mathrm{a.u.}]} \qquad (II)$$

where r(alk) denotes the rate of total alkane formation in the gas phase, ν(M) – moles of Pt and D – dispersion

$$\mathrm{H}_2/\mathrm{CO}_2 = \frac{r(\mathrm{H}_2)\left[\mathrm{mol\ min}^{-1}\right]}{r(\mathrm{CO}_2)\left[\mathrm{mol\ min}^{-1}\right]} \qquad (3)$$

Selectivity to alkanes (%)

$$S_{\mathrm{alk}} = \frac{\nu(\mathrm{C}_{\mathrm{alkanes}})}{\nu(\mathrm{C}_{\mathrm{in\ gas}})}\times 100\% \qquad (4)$$

Acknowledgements

The Academy of Finland in collaboration with the North European Innovative Energy Research Programme (N-Inner) and the Graduate School in Chemical Engineering (GSCE) and Fortum Foundation are gratefully acknowledged for financial support. In addition the COST-Action CM0903 (UbioChem) as well as the Bio4Energy programme in Sweden are acknowledged. The authors gratefully acknowledge the funding of the European Union Seventh Framework Programme (FP7/2007-2013) within the project SusFuelCat under grant agreement no. 310490 (http://www.susfuelcat.eu). B.H. and B.E. acknowledge the funding of the German Research Council (DFG), which supports the Cluster of Excellence "Engineering of Advanced Materials" and the German academic exchange service (DAAD). The work is a part of the activities of Process Chemistry Centre (PCC) financed by Åbo Akademi University.

References

1 *Thermochemical Conversion of Biomass to Liquid Fuels and Chemicals*, ed. M. Crocker, RSC Publishing, 2010.
2 C.-H. Zhou, X. Xia, C.-X. Lin, D. S. Tonga and J. Beltramini, *Chem. Soc. Rev.*, 2011, **40**, 5588–5617.
3 J. C. Serrano-Ruiz, R. Luque and A. Sepulveda-Escribano, *Chem. Soc. Rev.*, 2011, **40**, 5266–5281.
4 J. W. Shabaker, G. W. Huber, R. R. Davda, R. D. Cortright and J. A. Dumesic, *Catal. Lett.*, 2003, **88**, 1–8.
5 R. R. Davda, J. W. Shabaker, G. W. Huber, R. D. Cortright and J. A. Dumesic, *Appl. Catal., B*, 2003, **43**, 13–26.
6 G. W. Huber, J. W. Shabaker and J. A. Dumesic, *Science*, 2003, **300**, 2075–2077.
7 J. W. Shabaker, G. W. Huber and J. A. Dumesic, *J. Catal.*, 2004, **222**, 180–191.
8 G. W. Huber, J. W. Shabaker, S. T. Evans and J. A. Dumesic, *Appl. Catal., B*, 2006, **62**, 226–235.
9 X. Chu, J. Liu, B. Sun, R. Dai, Y. Pei, M. Qiao and K. Fan, *J. Mol. Catal. A: Chem.*, 2011, **335**, 129–135.
10 J. Liu, B. Sun, J. Hu, Y. Pei, H. Li and M. Qiao, *J. Catal.*, 2010, **274**, 287–295.
11 M. F. D'Angelo, V. Ordomsky, V. Paunovic, J. van der Schaaf, J. C. Schouten and T. A. Nijhuis, *ChemSusChem*, 2013, **6**, 1708–1716.
12 R. R. Soares, D. A. Simonetti and J. A. Dumesic, *Angew. Chem., Int. Ed.*, 2006, **45**, 3982–3985.

13 K. Lehnert and P. Claus, *Catal. Commun.*, 2008, **9**, 2543–2546.
14 G. Wen, Y. Xu, H. Ma, Z. Xu and Z. Tian, *Int. J. Hydrogen Energy*, 2008, **33**, 6657–6666.
15 E. L. Kunkes, R. R. Soares, D. A. Simonetti and J. A. Dumesic, *Appl. Catal., B*, 2009, **90**, 693–698.
16 P. D. Vaidya and A. E. Rodrigues, *Chem. Eng. Technol.*, 2009, **32**, 1463–1469.
17 A. Wawrzetz, B. Peng, A. Hrabar, A. Jentys, A. A. Lemonidou and J. A. Lercher, *J. Catal.*, 2010, **269**, 411–420.
18 A. O. Menezes, M. T. Rodrigues, A. Zimmaro, L. E. P. Borges and M. A. Fraga, *Renewable Energy*, 2011, **36**, 595–599.
19 D. Ö. Özgür and B. Z. Uysal, *Biomass Bioenergy*, 2011, **35**, 822–826.
20 A. V. Kirilin, A. V. Tokarev, L. M. Kustov, T. Salmi, J.-P. Mikkola and D. Yu. Murzin, *Appl. Catal., A*, 2012, **435–436**, 172–181.
21 T. Jiang, T. Wang, L. Ma, Y. Li, Q. Zhang and X. Zhang, *Appl. Energy*, 2012, **90**, 51–57.
22 G. W. Huber, R. D. Cortright and J. A. Dumesic, *Angew. Chem., Int. Ed.*, 2004, **43**, 1549–1551.
23 Y. Xu, Z. Tian, G. Wen, Z. Xu, W. Qu and L. Lin, *Chem. Lett.*, 2006, **35**, 216–217.
24 A. Tanksale, C. H. Zhou, J. N. Beltramini and G. Q. Lu, *J. Inclusion Phenom. Macrocyclic Chem.*, 2009, **65**, 83–88.
25 A. V. Kirilin, A. V. Tokarev, E. V. Murzina, L. M. Kustov, J.-P. Mikkola and D. Yu. Murzin, *ChemSusChem*, 2010, **3**, 708–718.
26 Q. Zhang, T. Wang, B. Li, T. Jiang, L. Maa, X. Zhang and Q. Liu, *Appl. Energy*, 2012, **97**, 509–513.
27 R. D. Cortright, R. R. Davda and J. A. Dumesic, *Nature*, 2002, **418**, 964–967.
28 Z. Tang, J. Monroe, J. Dong, T. Nenoff and D. Weinkauf, *Ind. Eng. Chem. Res.*, 2009, **48**, 2728–2733.
29 B. Roy, K. Loganathan, H. N. Pham, A. K. Datye and C. A. Leclerc, *Int. J. Hydrogen Energy*, 2010, **35**, 11700–11708.
30 A. V. Tokarev, A. V. Kirilin, E. V. Murzina, K. Eränen, L. M. Kustov, D. Yu. Murzin and J.-P. Mikkola, *Int. J. Hydrogen Energy*, 2010, **35**, 12642–12649.
31 N. Li and H. Huber, *J. Catal.*, 2010, **270**, 48–59.
32 R. R. Davda, J. W. Shabaker, G. W. Huber, R. D. Cortright and J. A. Dumesic, *Appl. Catal., B*, 2005, **56**, 171–186.
33 R. R. Davda and J. A. Dumesic, *Angew. Chem., Int. Ed.*, 2003, **42**, 4068–4071.
34 G. W. Huber, J. Chheda, C. B. Barrett and J. A. Dumesic, *Science*, 2005, **308**, 1446–2079.
35 N. Luo, X. Fu, F. Cao, T. Xiao and P. Edwards, *Fuel*, 2008, **87**, 3483–3489.
36 Y. Guo, M. U. Azmat, X. Liu, Y. Wang and G. Lu, *Appl. Energy*, 2012, **92**, 218–223.
37 K. Murata, T. Isao and M. Inaba, *React. Kinet. Catal. Lett.*, 2008, **93**, 59–66.
38 D. A. Simonenti, E. L. Kunkes and J. A. Dumesic, *J. Catal.*, 2007, **247**, 298–306.
39 E. L. Kunkes, D. A. Simonett, J. A. Dumesic, W. D. Pyrz, L. E. Murillo, J. G. Chen and D. J. Buttrey, *J. Catal.*, 2008, **260**, 164–177.
40 D. L. King, L. Zhang, G. Xia, A. M. Karim, D. J. Heldebrant, X. Wang, T. Peterson and Y. Wang, *Appl. Catal., B*, 2010, **99**, 206–213.
41 B. Meryemogl, A. Hesenov, S. Irmak, O. M. Atanur and O. Erbatur, *Int. J. Hydrogen Energy*, 2010, **35**, 12580–12587.
42 L. Zhang, G. Xia, Y. Yang, D. Heldebrant, D. King, Y. Wang and L. F. Allard, *Microsc. Microanal.*, 2010, **16 (Suppl. 2)**, 1428–1429.
43 L. Zhang, A. M. Karim, M. H. Engelhard, Z. Wei, D. L. King and Y. Wang, *J. Catal.*, 2012, **287**, 37–43.
44 A. C.-C. Chang, R. F. Louh, D. Wong, J. Tseng and Y. S. Lee, *Int. J. Hydrogen Energy*, 2011, **36**, 8794–8799.
45 X. Wang, N. Li, L. D. Pfefferle and G. L. Haller, *Catal. Today*, 2009, **146**, 160–165.
46 X. M. Wang, N. Li, J. A. Webb, L. D. Pfefferle and G. L Haller, *Appl. Catal., B*, 2010, **101**, 21–30.
47 X. M. Wang, N. Li, L. D. Pfefferle and G. L. Haller, *J. Phys. Chem. C*, 2010, **114**, 16996–17002.
48 X. M. Wang, N. Li, C. Wang, W. R. Swchartz, S. Lim, T. Fadel, L. D. Pfefferle and G. L. Haller, *ACS Catal.*, 2012, **2**, 1480–1486.
49 T.-W. Kim, H.-D. Kim, K.-E. Jeong, H.-J. Chae, S.-Y. Jeong, C.-H. Lee and C.-U. Kim, *Green Chem.*, 2011, **13**, 1718–1728.
50 H.-D. Kim, H. J. Park, T.-W. Kim, K.-E. Jeong, H.-J. Chae, S.-Y. Jeong, C.-H. Lee and C.-U. Kim, *Int. J. Hydrogen Energy*, 2012, **37**, 8310–8317.
51 H.-D. Kim, H. J. Park, T.-W. Kim, K.-E. Jeong, H.-J. Chae, S.-Y. Jeong, C.-H. Lee and C.-U. Kim, *Catal. Today*, 2012, **185**, 73–80.
52 R. M. Ravenelle, J. R. Copeland, W.-G. Kim, J. C. Crittenden and C. Sieverse, *ACS Catal.*, 2011, **1**, 552–561.
53 F. Rodríguez-Reinoso and A. Sepúlveda-Escribano, Chapter 9 – Porous Carbons in Adsorption and Catalysis, *Handbook of Surfaces and Interfaces of Materials*, 2001, 309355.
54 V. F. Surobikin, G. V. Plaxin, V. A. Semikolenov, V. A. Likholobov and I. J Tiunova, *US patent, US4978649*, 1990.
55 Y. I. Yermakov, V. F. Surobikin, G. V. Plaxin, V. A. Semikolenov, V. A. Likholobov, A. L. Chuvilin and S. V. Bogdanov, *React. Kinet. Catal. Lett.*, 1987, **33**, 435–440.
56 I. L. Simakova, O. Simakova, A. V. Romanenko and D. Yu. Murzin, *Ind. Eng. Chem. Res.*, 2008, **47**, 7219–7225.
57 O. A. Simakova, P. A. Simonov, A. V. Romanenko and I. L. Simakova, *React. Kinet. Catal. Lett.*, 2008, **95**, 3–12.
58 I. V. Deliy, I. L. Simakova, N. Ravasio and R. Psaro, *Appl. Catal., A*, 2009, **357**, 170–177.
59 L. B. Okhlopkova, A. S. Lisitsyn, V. A. Likholobov, M. Gurrath and H. P. Boehm, *Appl. Catal., A*, 2000, **204**, 229–240.
60 O. P. Taran, E. M. Polyanskaya, O. L. Ogorodnikova, C. Descorme, M. Besson and V. N. Parmon, *Catalysis in Industry*, 2010, **2**, 381–386.
61 V. Presser, M. Heon and Y. Gogotsi, *Adv. Funct. Mater.*, 2011, **21**, 810–833.
62 M. Schmirler, T. Knorr, T. Fey, A. Lynen, P. Greil and B. J. M. Etzold, *Carbon*, 2011, **49**, 4359–4367.
63 M. Schmirler, F. Glenk and B. J. M. Etzold, *Carbon*, 2011, **49**, 3679–3686.

64 A. Schlange, A. R. dos Santos, B. Hasse, B. J. M. Etzold, U. Kunz and T. Turek, *J. Power Sources*, 2012, **199**, 22–28.
65 L. Borchardt, F. Hasché, M. R. Lohe, M. Oschatz, F. Schmidt, E. Kockrick, C. Ziegler, T. Lescouet, A. Bachmatiuk, B. Büchner, D. Farrusseng, P. Strasser and S. Kaskel, *Carbon*, 2012, **50**, 1861–1870.
66 A. Silvestre-Albero, S. Rico-Francés, F. Rodríguez-Reinoso, A. M. Kern, M. Klumpp, B. J. M. Etzold and S.-J. Alberro, *Carbon*, 2013, **59**, 221–228.
67 T. Knorr, P. Heinl, J. Schwerdtfeger, C. Körner, R. F. Singer and B. J. M. Etzold, *Chem. Eng. J.*, 2012, **181–182**, 725–733.
68 F. Glenk, T. Knorr, M. Schirmer, S. Gütlein and B. Etzold, *Chem. Eng. Technol.*, 2010, **33**, 698–703.
69 J. C. Palmer, A. Llobet, S.-H. Yeon, J. E. Fischer, Y. Shi, Y. Gogotsi and K. E. Gubbins, *Carbon*, 2010, **48**, 1116–1123.
70 R. Rajagopalan, A. Ponnaiyan, P. J. Mankidy, A. W. Brooks, B. Yi and H. C. Foley, *Chem. Commun.*, 2004, 2498–2499.
71 A. Corma, *Chem. Rev.*, 1995, **95**, 559–614.
72 P. Serp, and J. L. Figueiredo, *Carbon Materials for Catalysis*, John Wiley & Sons 2009.
73 T. J. Bandosz, J. Jagiello and J. A. Schwarz, *Anal. Chem.*, 1992, **64**, 891.
74 J. W. Shabaker, D. A. Simonetti, R. D. Cortright and J. A. Dumesic, *J. Catal.*, 2005, **231**, 67–76.
75 Y. T. Kim, J. A. Dumesic and G. W. Huber, *J. Catal.*, 2013, **304**, 72–85.
76 T. Jiang, Q. Zhang, T.-J. Wang, Q. Zhang and L.-L. Ma, *Energy Convers. Manage.*, 2012, **59**, 58–65.
77 R. Van Hardeveld and F. Hartog, *Surf. Sci.*, 1969, **15**, 189–230.
78 A. Ciftci, B. Peng, A. Jentys, J. A. Lercher and E. J. M. Hensen, *Appl. Catal., A*, 2012, **431–432**, 113–119.
79 D. A. Boga, R. Oord, A. M. Beale, Y.-M. Chung, P. C. A. Bruijnincx and B. M. Weckhuysen, *ChemCatChem*, 2013, **5**, 529–537.
80 Y.-G. Wang, L. Cheng, F. Li, H.-M. Xiong and Y.-Y. Xia, *Chem. Mater.*, 2007, **19**, 2095–2101.
81 O. Hofstadt and K. Kartte, *Patent EP0193889*, 1986.
82 B. Hasse, F. Reißner, C. Dicenta, P. Hausmann and B. J. M. Etzold, Carbide-derived carbon (TIC-CDC) as model catalyst support – an exemplary study, *15-th International Congress on Catalysis 2012*, Munich, Germany, 2012.
83 P. Brunelle, *Stud. Surf. Sci. Catal.*, 1979, **3**, 211–232.
84 X. Hao, S. Barnes and J. R. Regalbuto, *J. Catal.*, 2011, **279**, 48–65.
85 X. Hao, L. Quach, J. Korah, W. A. Spieker and J. R. Regalbuto, *J. Mol. Catal. A: Chem.*, 2004, **219**, 97–107.
86 R. L. Manfro, T. P. M. D. Pires, N. F. P. Ribeiro and M. M. V. M. Souza, *Catal. Sci. Technol.*, 2013, **3**, 1278–1287.
87 A. V. Kirilin, A. V. Tokarev, H. Manyar, C. Hardacre, T. Salmi, J.-P. Mikkola and D. Yu. Murzin, Aqueous phase reforming of xylitol over Pt–Re bimetallic catalyst: effect of the Re addition *Catal. Today*, 2013http://dx.doi.org/10.1016/j.cattod.2013.09.020.